Regulation of the Liquid–liquid Phase-Separated Droplets of Biomacromolecules by Butterfly-Shaped Gold Nanomaterials

Tomohiro Nobeyama*[a], Koji Takata[b,c], Megumi Mori[d], Tatsuya Murakami[b], and Kentaro Shiraki[a]

[a] Faculty of Pure and Applied Sciences, University of Tsukuba, 1-1-1 Tennodai, Tsukuba, Ibaraki 305-8573, Japan

[b] Graduate School of Engineering, Toyama Prefectural University, 5180 Kurokawa, Imizu, Toyama 939-0398 Japan

[c] Human Life Technology Research Institute, Toyama Industrial Technology Research and Development Center, 35-1 Iwatakeshin, Nanto, Toyama 939-1503, Japan

[d] Faculty of Agriculture, Kyoto University, Sakyo-ku, Kyoto 606–8502 Japan

KEYWORDS Nanotechnology, Liquid–liquid Phase Separation, Gold nanobutterfly

ABSTRACT: Liquid–liquid phase-separated (LLPS) droplets play key roles in regulating protein behaviors, such as enzyme compartmentalization, stress response, and disease pathogenesis, in living cells. The manipulation of the droplet formation/deformation dynamics is the next target of nano-biotechnology, although the required nanodevices for controlling the dynamics of liquid–liquid phase separation, LLPS, have not been invented. Here, we propose a butterfly-shaped gold nanobutterfly (GNB) as a nanodevice for manipulating the droplet-formation/deformation dynamics of LLPS. GNBs are moderate, symmetrical gold nanomaterials (average diameter = ~30 nm) bearing two concaves and resembling a butterfly. Their growth process is analyzed *via* their time-lapse electroscopic images and time-lapse ultraviolet/visible/near-infrared (NIR) spectroscopy, as well as the application of solution additives in protein science. These nanomaterials are synthesized *via* the seed-mediated method with an efficiency of ~70%. Interestingly, the GNBs stabilized the LLPS droplet of adenosine triphosphate (ATP)/poly-L-lysine, whereas other two gold nanoparticles with different shapes (spherical and rod-shaped) did not, indicating that the concave of the GNBs interacts with the precursor of the droplets. The NIR-laser irradiation of the GNBs facilitates the on-demand deformation of the droplets *via* the localized-heat effect. This butterfly-shaped nanodevice represents a future strategy for manipulating the dynamics of LLPS.

Introduction

The control of small structures in living cells is among the most attractive methodologies in life science and nanotechnology[1-2]. For example, recent progress in cellular biology reveals that the small droplet structures that are formed by liquid–liquid phase separation (LLPS) determine cell behaviors[3-5]. The dynamic LLPS of biomacromolecules generates temporal compartmentalized space[6], as well as accumulated substrates and enzymes in the droplet, to ensure the effectiveness of the tandem reaction process[7-8] and/or increase the enzyme activity[9]. LLPS droplets are greatly observed in transcription, as well as in the stress responses of mammals[10-11] and plants[12]. Droplet formation is also related to the pathological role of proteins related to neurodegenerative diseases, such as Alzheimer's disease[13-14]. Thus, the manipulation of the formation/deformation of liquid–liquid phase-separated (LLPS) droplets would be profitable for next-generation targeting in cell engineering.

The extant theoretical and experimental studies have advanced the fundamental knowledge of the dynamics of the droplet-assembly process. Several studies have indicated that immature droplets or a protein assembly accumulate and dissociate in the cytosol and that these dynamic behaviors cause the formation and deformation of mature droplets[15-19]. Those studies revealed that interfering with small, immature droplets is an essential part of manipulating the LLPS dynamics. Since the precursor of droplets is very small, utilizing a small nanomaterial-produced manipulator would be among the best methodologies for manipulating the LLPS dynamics.

The surface engineering of nanomaterials benefits target-selective delivery by engineering the "nano–bio interface" where will be the contact point between a nanomaterial and target[20]. Classically, targets, such as a specific cell surface or cytosol, are considerably larger (>1 μm) than nanomaterials (several tens of nm). Under such conditions, the dominant property of the nano–bio interface is determined by the entire properties of the nanomaterial surface, including its total surface charge, hydrophilicity/hydrophobicity, and/or total radius. Conversely, if the target is as small as the nanomaterial, the detailed surface shape, *e.g.*, the numbers of convexes/concaves or radius of the material surface, cannot be neglected[21-25]. Therefore, imparting skillfully developed characteristics is key to designing manipulators for small structures.

Nanotechnology-driven cell engineering has contributed various kinds of nanomaterials, such as gold[26-27], and silver[28] nanomaterials, as cellular control manipulators. Particularly, gold nanomaterials are the most widely utilized because of their high stability[29-30], their low side effects, the ease of handling their synthesis process[31-32], and their shape-dependent optical properties [33]. For example, gold nanorods (GNRs), which are anisotropic rod-shaped gold nanomaterials, absorb near-infrared (NIR) light and convert it into local heat. Since NIR lasers penetrate cell components and water, they are utilized for heat-induced gene regulation, in drug-delivery systems, and for cancer therapy[33-34].

Gold nanoparticles are generally synthesized *via* the seed-mediated growth method[35]. Typically, very small gold nanomaterial (seed) that is prepared separately or *in situ*[36] are mixed with surfactants, Au^{3+} ions, and reductants, after which they are kept for hours. Subsequently, the Au^{3+} ions are reduced into Au^{+} in the solution, and the colliding Au^{+} ions with the seed or growing nanomaterial reduces into Au atoms on the surface[36]. Owing to the randomized collision process, almost all the previous gold nanomaterials exhibit symmetry, such as spherical, rod-like, and triangular shapes, or no symmetry, such as nanourchin[37]. As far as we know, only a few types of moderately symmetrical non-rod-like gold nanomaterials with high efficiency are known; they include gold nanoflowers, gold nanostar, and DNA-programable overgrowth of GNRs[38-41].

The mechanistic insights into synthesizing anisotropic gold nanomaterials have been explored for decades. Recent progress indicated that surfactants and silver ions inhibited the typical crystal facet of growing gold nanomaterial, although the detailed mechanisms are still controversial[42-44]. Thus, improving the methodology for fabricating nanodevices with moderate symmetries has not been sufficiently investigated because of the limited mechanistic insights, and this represents a hurdle to the development of biocompatible nanodevices for controlling small nanostructures in a cell.

Herein, we report the synthesis and utilization of a new nanomaterial (gold nanobutterflies, GNBs). GNBs exhibit a butterfly-like shape including two concaves in the opposite sites of the NPs without a larger convex at the top and bottom. The complex shape was formed by combining solution additives that have been used in the field of protein science for the semi-quantified analysis of weak interactions in very complicated systems[45]. Concave GNBs exhibit a similar size to those of immature droplets. The adoption of additive effects represents a universal methodology for discussing the formation pathways of other anisotropic gold nanomaterials. We also demonstrated the GNBs in the regulation of the formation/deformation dynamics of model LLPS droplets.

Experimental Section

Results and Discussions

Synthesis of GNBs

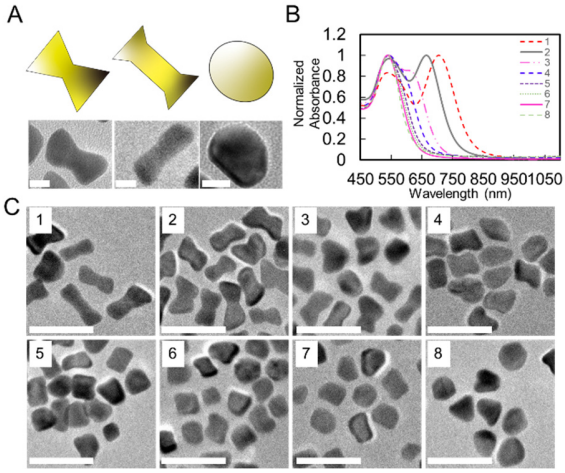

Figure 1. Structure of the synthesized GNBs. (A) Schematics of the nanoparticles: GNBs (left), GNRs (middle) and sphere-shaped gold nanoparticles (right). Scale bar = 10 nm (B) Typical ultraviolet/visible (UV/VIS)/NIR spectra of the synthesized nanoparticles. Each sample number indicates the final concentration of L-ascorbic acid (L-AA), *i.e.*,1.6 mM, 3.2 mM, 6.4 mM, 12.8 mM, 25.6 mM, 51.2 mM, 91.6 mM, and 164 mM, respectively. (C) Representative transmission electron microscopy (TEM) image of each nanoparticle. No. 2 indicates the synthesis of gold nanobutterflies (GNBs). Scale bar = 50 nm.

The GNBs were synthesized *via* the seed-mediated growth approach, which has been used for various gold nanoparticles including GNRs[35]. Briefly, a gold seed solution was first prepared *via* rapid reductions by $NaBH_4$. Thereafter, the freshly prepared seed solution was added to the growth solution for crystal growth. The solution contained $HAuCl_4$ as the gold source, $AgNO_3$ as an additive to modulate the crystal growth, L-AA as a reductant, and surfactants. We observed that the surfactant solution containing benzyldimethyldodecylammonium chloride (BDAC) and hexadecyltrimethylammonium bromide (CTAB) in a 2:1 ratio, as well as 0.1 M total surfactant, was suitable for the highly efficient synthesis of GNBs. Similar compositions have been applied to the synthesis of rod-shaped GNRs, but this one has never

been established because of its high sensitivity to the shape (vide infra). However, we observed that this unsteady condition was key to modulating asymmetry if adequately improved.

$HAuCl_4$(aq), $AgNO_3$(aq), the freshly prepared L-ascorbic acid (L-AA)(aq), and the seed solution were added to the surfactant mixture (Experimental Section). Figure 1A shows the structure of the GNB. By changing the amount of L-AA, the UV/VIS/NIR spectra (Figure 1B) and TEM images of the nanomaterials also changed (Figure 1C). At a lower concentration of L-AA, the UV/VIS/NIR spectrum exhibited a strong absorbance peak (at the NIR region) and another relatively weak peak at the visible area derived from the plasmon on nanomaterial surfaces. This is a typical characteristic of the GNR spectrum. At an appropriate concentration of L-AA, the UV/VIS/NIR peaks displayed two distinguished peaks at around 550 nm and 650 nm. Both peaks exhibited the same intensity, and this represents a characteristic of GNBs.

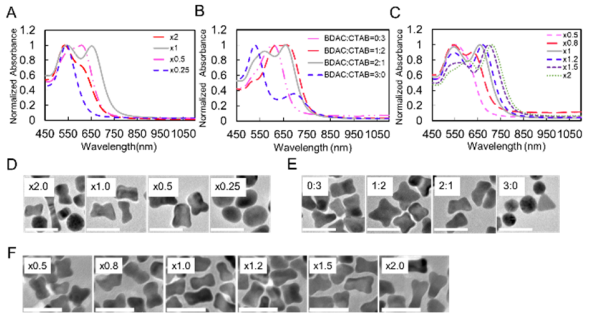

Figure 2. Effects of the silver ions and surfactants on GNB synthesis. (A)Typical UV/VIS/NIR spectra of the NPs with silver ions. Relative concentration of the silver ions is shown on the right side of the graph: x1 indicates that 0.04 mM silver ions is the final concentration. (B) Typical UV/VIS/NIR spectra of the NPs that were synthesized with various surfactant ratios. Final total concentration of the surfactants is 0.1 M. Each surfactant ratio is shown on the right side of the graph. (C) Typical UV/VIS/NIR spectra of the NPs with various concentrations of the BDAC:CTAB = 2:1 mixture. The relative concentration of the mixture is shown on the right side of the graph. x1 indicates that 0.1 M is the final concentration. (D)–(F) Typical TEM images of the NPs synthesized in Figure (A),(B), and (C), respectively. Scale bar = 50 nm

The ceiling of the GNBs was relatively plane (Figure S1). The comparison of the scanning electron microscopy (SEM) images of gold nanourchins and the GNBs indicated that the ceiling of GNB did not exhibit a large convex. This is dissimilar to the convex NRs or nanocubes[46-47]. We observed that 80 µL of 400 mM L-AA(aq) was ideal for the synthesis of GNBs. The concentration of L-AA(aq) represented a relatively higher condition than the usual experimental condition for synthesizing GNRs, although the GNBs exhibited a uniform shape[35, 48]. The counting of the NPs in the TEM images revealed that the GNB ratio was ~70% under our condition (Figure S2). Under low concentrations of L-AA, the GNBs could not be synthesized as the main product; rather, the GNRs were generated (Figures 1 and S2). A higher concentration of L-AA increased and decreased the ratios of the sphere-shaped-gold-nanoparticles (refered to as GNPs in this paper) and GNB, respectively (Figures 1 and S2). Based on the experiments discussed above, the amount of L-AA(aq) was fixed at 80 µL. The typical morphological characteristic of each kind of nanomaterial is also shown in Figure S2.

Mechanism of GNB Synthesis

We separately investigated the amount of Ag^+ ions, surfactant composition, and total surfactant condition (Figure 2). The UV/VIS/NIR spectra (Figures 2A–2C) and TEM images (Figures 2D–2F) were obtained with variable amounts of Ag^+ ions, two surfactant ratios, and surfactant mixture concentrations. For the Ag^+ ion, any conditions without first optimizing the concentrations demonstrated reduced efficiency of GNB synthesis (Figures 2A and 2D). The 0.25-fold-ratio condition only produced GNPs, while the 0.5-fold and 2-fold conditions yielded GNB with <55% efficiency (Figure S3). The synthesized nanomaterials did not exhibit a uniform shape under these conditions. The surfactant compositions significantly changed the shape of the nanomaterial (Figures 2B, 2E, and S3). Without BDAC, a few GNBs were synthesized under our condition. When the BDAC:CTAB = 1:2 ratio was used, cross-shaped nanomaterials were observed at ~25% (Figure S3). Notably, the synthesis of concave nanoparticles with rotational symmetry, such as nanostar synthesis, was still challenging[40]. These data indicated the high potential of our system for synthesizing moderately symmetrical gold nanomaterial. Without CTAB, large and small percentages of GNPs and nanotriangles were observed (Figures 2B and S3). A suitable amount of Ag^+ ion was essential for shape uniformity, and the ratio of BDAC determined the modest symmetrical shape of the nanomaterials, such as a cross or butterfly shape.

Further, we changed the molar concentration of the surfactant mixtures from 0.5-fold to 2-fold in stages and monitored the changes in the UV/VIS/NIR spectra and morphology of the nanoparticles (Figures 2C and 2F). The 1-fold sample represents the original concentration for GNB synthesis. By increasing the concentration, the short-wavelength peak of the spectra reduced and shifted to the longer side. The characteristic long-wavelength peak was turned for observation at the surfactant concentration of over 0.8-fold; it shifted toward a longer wavelength as the concentration increased. The peak ratio of the short and long wavelengths was >1 until the surfactant concentration reached 1, and the peak intensity reversed under higher concentration conditions. The changes in the nanomaterial shape also corresponded to the spectra changes (Figures 2C and 2F). The GNB shapes were observed well under the one-fold conditions; higher and lower concentrations exhibited lower efficiencies for producing GNBs (Figure S3). These data indicated that the concentration of BDAC would affect the morphology of nanomaterials.

To gain insight into the mechanism of GNBs formation, we first performed time-lapse TEM imaging and time-resolved UV/VIS/NIR absorption analysis in the GNBs synthesis (Figures 3A and 3B). Figure 3A shows that the rod-like nanomaterial was formed within 1 h, and the wing part of

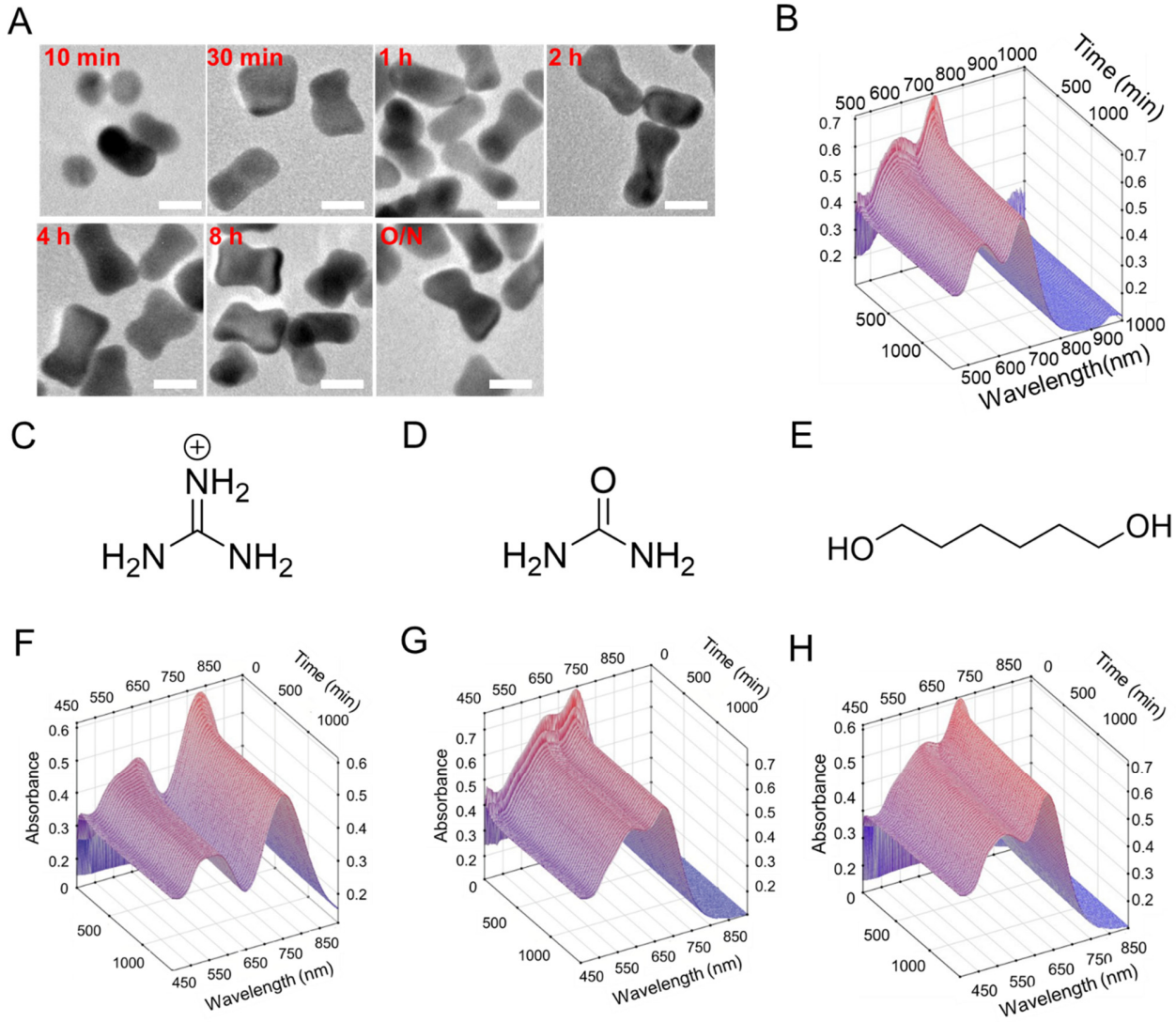

Figure 3. Analysis of the GNB-growth process in the presence of additives. (A) Time-lapse observation of the formation of GNB *via* TEM imaging. Scale bar = 20 nm. (B) Time-lapse measurement of the UV/VIS/NIR spectra during GNB formation. (C)–(E) Chemical structures of the additives: guanidine (C), urea (D), and 1,6 hexanediol (E). (F)–(H) Time-lapse measurement of the UV/VIS/NIR spectra in the nanoparticle-formation processes with 125 mM guanidine (F), urea (G), and 1,6 hexanediol (H)

the GNB matured over the subsequent several hours. The UV/VIS/NIR spectral change corresponded to the results of the TEM images (Figure 3B). Concretely, one strong NIR peak, which was typical of GNR, followed by another relatively weak one in the visible area, emerged. Afterward, both peaks shifted gradually toward the peak location of GNBs within ~10 h. These data indicate that the GNB-formation process comprised two steps, namely the rapid formation of the anisotropic shape and the gradual maturing into the butterfly shape.

Next, we tried to determine the origin of anisotropic formation of GNBs. We considered the following three hypotheses for GNB synthesis: (i) The interaction between the aromatic ring of BDAC and the cationic ions, such as Ag^+ and/or Au^+, would be essential. (ii) The hydrophobic interaction between the surfactant molecules modified the micelle shape that affected the growth of the nanomaterial. (iii) The hydrogen bonding from the surrounding water was essential to the shapes of the growing nanomaterial, and the surrounding ions, such as Ag^+ and surfactants, would modify the interaction of water and the reaction field or nanomaterial surface. To test these hypotheses, we strived to gain insight by using additives to inhibit one or two of the specific, weak interactions. Notably, small molecular-weight additives are widely used in the field of protein science or colloidal chemistry, where various kinds of weak interactions exist simultaneously in a target system, and they determine the behavior of such systems[45, 49].

We utilized the three representative additives for this analysis (Figures 3C, 3D, and 3E). Guanidine is a protein denaturant that can mainly inhibit cation–π and hydrophobic interactions[49-51]. Urea is another protein denaturant that can mainly inhibit hydrogen bonding and hydrophobic interaction[52]. Further, 1,6-hexanediol is a popular additive for demixing LLPS droplets; it can mainly inhibit hydrophobic interactions[53]. The interactions can be identified by growing gold particles in a solution containing these additives (Figure S4). We dissolved these additives consecutively in a 125 mM concentration in advance and conducted the GNB synthesis before measuring the time-lapse spectra to gain insight into the growth process of GNBs (Figures 3F, 3G, and 3H). The synthesis experiments with additives obtained a clear result. For the guanidine batch, both peaks exhibited rapidly changing long-wavelength ranges (Figure 3F). The decrease with time followed the same trend as that of the control experiment. The shape of the final UV/VIS/NIR spectra indicated the rod-like shape of the nanoparticles. Strong and weak peaks were observed in the NIR and Vis regions, respectively. For the urea samples, the peak largely reflected the synthesis of GNBs (Figure 3G). The cave between every two peaks was relatively shallow in the final UV/VIS/NIR spectra, although this change was not as rapid as that observed for the guanidine sample. For the 1,6-hexanediol samples, the time-lapse and final spectra did not change essentially compared with those of the control experiment (Figure 3H). These data indicated that the cation–π interaction between Ag^+ or Au^+ and the aromatic ring of BDAC was key to synthesizing the GNBs formation, and this interaction was key to the initial step of the synthesis.

Detailed Observation of the Effects of the Additives

To reveal additional information on the effects of the additives on the morphology of the nanomaterial, we changed the concentrations of the additives and analyzed their UV/VIS/NIR spectra (Figures 4A–4C) and TEM images (Figures 4D–4F) under each condition. The guanidine-containing samples did not exhibit the characteristic of the GNBs: the two peaks with almost the same intensities around 550 nm and 650 nm (Figure 4A). The UV/VIS/NIR spectra of the sample containing guanidine were the same as those of GNRs, with a strong and weak peak at around 750 nm and 570 nm, respectively. The TEM images indicated that a large part of the nanomaterial was longer and exhibited a relatively high aspect ratio (Figure 4D). The peak shift was reasonable as the GNRs were generated from the surface plasmon of the GNRs[35] even though some small horns existed on the edges[38]. The shape of the nanomaterial exhibited low uniformity in the 62.5 mM guanidine and high uniformity in the 250 mM and 125 mM guanidine. The maturing toward butterfly-like shapes was depicted in the urea and 1,6-hexanediol samples. Their UV/VIS/NIR sample did not change significantly at any concentration (Figures 4B and 4C). The caves of both peaks were shallow and deep in the urea and 1,6-hexanediol samples, respectively, but their peak positions and intensities did not change significantly compared with the case of the control samples. Dissimilar to the guanidine samples, a large part of the nanomaterials exhibited a GNB shape in the remaining two additive samples at all the concentrations (Figures 4E and 4F). Notably, in the 250 mM

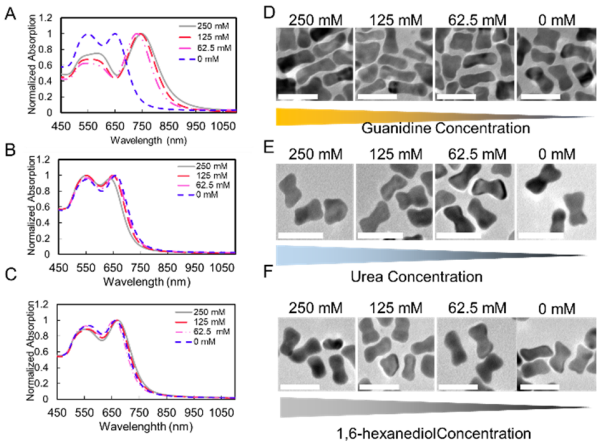

Figure 4. Detailed observation of effects of the additives. (A)–(C) UV/VIS/NIR spectra of the nanoparticles synthesized with various concentrations of guanidine (A), urea (B), and 1,6-hexanediol (C). Concentrations are shown in the upper right of the graphs. (D)–(F) TEM images of the NPs synthesized under the same conditions as those of Figures (A), (B), and (C), respectively. Scale bar = 50 nm

1,6-hexanediol samples, some of the GNBs exhibited relatively round-shaped edges. The hydrophobic interaction of the reagents determined the crystal growth direction of the gold nanomaterials at the late stage, and the inhibition of this interaction weakened the sharpness of the crystal edges of the GNBs.

These data revealed that the cation–π interactions played a major role in the growth of the butterfly-shaped NPs. Additionally, the hydrophobic interaction of the reagents, a large part of which was probably surfactants near the gold nanomaterial, was the minor determinant to accelerate the crystal growth of GNBs owing to the slight difference in the time-lapse spectrum with 125 mM urea (Figure 3G), as well as the morphological changes of the nanomaterials in 250 mM 1,6-hexanediol (Figure 4F and S5).

Based on the discussed data, we proposed the growth mechanism (Figure 5). The seed functioned as a core, as obtainable in other seed-mediated growth syntheses. The Ag^+ ions enabled the anisotropic growth of the gold nanomaterials, and the cation–π interaction between the metal ion and aromatic ring of BDAC determined the length of nanomaterials at the early stage. Afterward, the nanomaterials matured into GNBs in dozens of hours. This process is also related to the cation–π interactions between the metal ion and BDAC. We have a hypothesis that BDAC moderates the silver ion capping in the early stage to limit the anisorotopic rod-growth[42, 54] and in the late stage it somehow ss the GNBs wing formation, e.g., via accumulation of surfactants on the sides of nanomaterials. Silver ions induced rod shape as well known. BDAC would attract on the outer sides of maturing GNBs and prepend Ag^+- Au surface interaction via cation–π interaction. Larger silver ion concentration condition and larger surfactant concentration condition, where surface micelle did not form well, resulted in relatively larger ratio of GNRs due to the lack of well obstacle of Ag+-

Au interaction(Figure S3) BDAC:CTAB=2:1 condition have enough amount of BDAC in first step but it was no enough to block the side of growth nanomaterial well so that some of nanomatrials had cross shapes(Figure 2 and Figure S3) The detail investigation of the GNB-formation mechanism is beneficial to the optimization of the GNB shapes for controlling the formation of LLPS droplets.

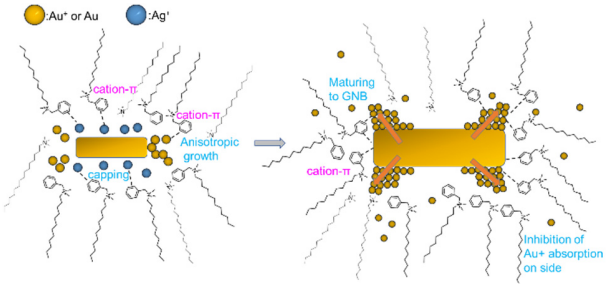

Figure 5. Schematic of the proposed mechanism of GNB formation and key noncovalent interactions. In the first step (left), the cation–π interaction between Ag^+ or Au^+ and BDAC determine the anisotropic one-direction growth. Inhibition of cation– π interaction caused an excessive increase in the aspect ratio. In the second step (right), the Au^+ ions accumulated on the typical facet of the nanoparticles *via* the cation–π interaction between BDAC and Au^+. The location of BDAC was affected by the hydrophobic interaction between the surfactants as shown in figure S3, as well as the effect on the crystal growth of the nanoparticles into GNB

Controlling the Formation of Model LLPS Droplets

The unique shape of GNBs allowed us to come up with an idea to apply them to control the formation/deformation dynamics of LLPS droplets (Figures 6, S7, and S8). The LLPS droplets are small, sphere structures that were derived from the phase separation of biomacromolecules, such as proteins, DNA, and RNA with other biomacromolecules and/or small molecules. We investigated the interference of GNBs in the formation of the LLPS droplets. As a model system, we selected the adenosine triphosphate (ATP)/poly-l-lysine droplets, which is a widely utilized model to study the LLPS between protein and nucleic acid[55-57]. First, we prepared three types of nanomaterials with the same reagents with different concentrations, namely, GNBs, GNPs, and GNRs, to determine the local-size effect of the nanomaterials on droplet formation. Each nanoparticle was first washed with and dispersed in 100 mg/mL poly-L-lysine aqueous solution at a *ca.* 1 mg/mL concentration of the nanomaterial. Each dispersion and 1 M ATP solution were mixed to obtain a 1:4 molar ratio of the lysine structure and ATP molecule. Notably, this condition did not yield any droplets without the nanomaterials (Figure S7).

A black aggregation of the GNPs deposited, but the GNRs and GNBs did not aggregate in the solution (Figure 6A). The GNR samples exhibited small, visible droplets, and GNRs were not included in the droplets. Conversely, the GNBs produced mature droplets, which were larger than those of the other samples. The microscopic images indicated that some parts of the GNBs were incorporated in the droplets (Figures 6B and S7). To check the droplet likeness of the condensates under each condition, we applied the effects of the additive ions to dissolve them. The driving force of the poly-L-lysine droplets was the electrostatic interaction; thus, the addition of NaCl, an inhibitor of electrostatic interaction, can drive the dissolution of the droplets[56].

We mixed the condensate dispersants and NaCl solution at each concentration in a 1:1 volume ratio (Figure S8). The droplets, induced by GNBs (GNB droplets), were dissolved

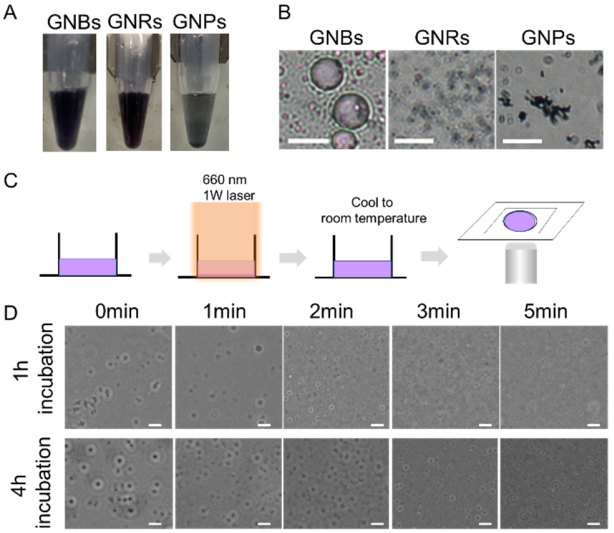

Figure.6. Incorporation of GNBs into LLPS droplets. (A) Colloidal stability and instability of nanoparticles with ATP/Poly-L-lysine droplets (B) Typical microscopic images of the droplets with nanoparticles. GNPs were aggregated in the picture. (C) Experimental scheme of droplet deformation assay by using laser irradiation (D)Typical microscopic image of the droplets with GNBs. Laser irradiation time were shown above each picture. Incubation times on silicon chamber were shown in left side of picture. Scale bar = 10 μm

at >0.63 M final concentration of NaCl. Contrarily, the GNR condensates remained a little, and the GNP condensates still maintained a large aggregation even at a 2.5 M final concentration of NaCl. These data indicated that the GNB condensates exhibited droplet tendencies, while the GNP condensates tended toward aggregation.

We also attempted the on-demand control of the reverse droplet deformation process with the photothermal effects of the gold nanomaterial[58]. We previously reported a gold-nanomaterial-driven system for facilitating the photothermal control of structure formation[59]. We adopted a similar photothermal system to manipulate droplet deformation (Figure 6C). We dropped 50 uL of the GNB condensate dispersant in 96-well plates and irradiated them with a 660-nm laser. After cooling down, the irradiated dispersant was dropped on a silicon chamber and kept for 1 h or 4 h to allowthe droplets settled onto the bottom of each chamber(Figure6D). NIR-laser irradiation for 1 min kept the droplets; however, ≥2 min irradiation significantly dispersed the droplet structures. After 4 h of incubation in the chamber, the 1 min- and 2 min-irradiated samples appeared

to recover their condensate structures to some extent. This result indicated two things. First, the condensate exhibited a droplet tendency. The slow movement of the macromolecule at a high concentration induced LLPS after the incubation. Second, the required laser power for driving droplet deformation would be lower than the power for decomposition of poly-L-lysine, which would occur in the 3 min-irradiated samples. Although the local heating of phase-separated structures was performed using the photothermal effect derived from the usual surface plasmon of gold nanomaterial[58-60], this study is the first demonstration of photocontrol of the LLPS formation. Recently, LLPS droplets as well as other phase separated structures were considered as a target of drug discovery (ref), however, their targeting and modulation have been still challenging. Thus, GNBs are the first nanomaterial capable of them.

We assumed that the modest size and number of concaves on the GNB surface would play critical roles in visible droplet formation. The stabilized, invisible small droplets from the GNB surface enabled the aggregation and growth to form the droplets. Contrarily, the convex shape of the GNRs and GNPs did not contribute to the formation of the droplets. The NIR-laser irradiation drove the dissolution of the visible droplet, although it might have driven its reformation (Figure 6). These observations indicated the significance of the local convex/concave in the occurrence/dispersion of LLPS in high concentration solutions, such as cytosol.

Conclusion

In summary, we report the synthesis of butterfly-shaped nanoparticles (GNBs) and discuss their synthesis mechanism *via* an additive-effect approach. The GNBs demonstrated the possibility of designing a nanodevice for interfering with the early stage of droplet formation and on-demand photodispersion of droplets *via* NIR-laser irradiation. The detailed investigation of the formation of moderately symmetrical nanoparticles represents an essential insight for other appropriate nanodevices for controlling small biological nanostructures, as well as the facet control of nanomaterial syntheses to produce additional sophisticated structures[46, 61].

Gold nanomaterials exhibit great possibilities in nanotechnology owing to their high stability, low toxicity, and optical properties. In this research, we revealed the first step for incorporating gold nanomaterial into droplets through a droplet formation mechanism using the local-size effect of GNBs. In the future, the formation/deformation, property, maturing, and inner enzymic reactions may be controlled with gold nanodevices.

ASSOCIATED CONTENT

Supporting Information. Supporting Information includes General information on materials, detailed explanation of experiments, and supporting figures. This material is available free of charge via the Internet at http://pubs.acs.org.

AUTHOR INFORMATION

Corresponding Author

* Tomohiro Nobeyama
Faculty of Pure and Applied Sciences, University of Tsukuba,
1-1-1 Tennodai, Tsukuba, Ibaraki 305-8573, Japan
E-mail: nobeyama.tomohiro.fu@u.tsukuba.ac.jp

Author Contributions

The manuscript was written through contributions of all authors. All authors have given approval to the final version of the manuscript.

Funding Sources

This study was supported by the KAKENHI of the Japan Society for the Promotion of Science (JSPS) to T.N. (19J14903) and T.N. (21J00852).

Acknowledgment

We are grateful for the kind support of Toyama Prefectural University, Kyoto University, and the University of Tsukuba. We are grateful for the academic and supportive atmosphere afforded by Kumano Dormitory at Kyoto University. We thank Hiroaki Soji and Dr. Takashi Sekiguchi for the SEM imaging of the nanomaterials.

We would like to thank Enago(www.enago.jp) for the English language review.

References

1. Newkirk, G. M.; de Allende, P.; Jinkerson, R. E.; Giraldo, J. P., Nanotechnology Approaches for Chloroplast Biotechnology Advancements. *Front Plant Sci* **2021,** *12*, 691295.
2. McNeil, S. E., Nanotechnology for the biologist. *J. Leukoc. Biol.* **2005,** *78* (3), 585-94.
3. Hyman, A. A.; Weber, C. A.; Julicher, F., Liquid-liquid phase separation in biology. *Annu. Rev. Cell Dev. Biol.* **2014,** *30*, 39-58.
4. Uversky, V. N., Recent Developments in the Field of Intrinsically Disordered Proteins: Intrinsic Disorder-Based Emergence in Cellular Biology in Light of the Physiological and Pathological Liquid-Liquid Phase Transitions. *Annu Rev Biophys* **2021,** *50*, 135-156.
5. Gomes, E.; Shorter, J., The molecular language of membraneless organelles. *J. Biol. Chem.* **2019,** *294* (18), 7115-7127.
6. Shin, Y.; Brangwynne, C. P., Liquid phase condensation in cell physiology and disease. *Science* **2017,** *357* (6357).
7. Strulson, C. A.; Molden, R. C.; Keating, C. D.; Bevilacqua, P. C., RNA catalysis through compartmentalization. *Nat. Chem.* **2012,** *4* (11), 941-6.
8. Aumiller, W. M., Jr.; Davis, B. W.; Hashemian, N.; Maranas, C.; Armaou, A.; Keating, C. D., Coupled enzyme reactions performed in heterogeneous reaction media:

experiments and modeling for glucose oxidase and horseradish peroxidase in a PEG/citrate aqueous two-phase system. *J. Phys. Chem. B* **2014,** *118* (9), 2506-17.
9. Crosby, J.; Treadwell, T.; Hammerton, M.; Vasilakis, K.; Crump, M. P.; Williams, D. S.; Mann, S., Stabilization and enhanced reactivity of actinorhodin polyketide synthase minimal complex in polymer-nucleotide coacervate droplets. *Chem. Commun. (Camb.)* **2012,** *48* (97), 11832-4.
10. Nott, T. J.; Petsalaki, E.; Farber, P.; Jervis, D.; Fussner, E.; Plochowietz, A.; Craggs, T. D.; Bazett-Jones, D. P.; Pawson, T.; Forman-Kay, J. D.; Baldwin, A. J., Phase transition of a disordered nuage protein generates environmentally responsive membraneless organelles. *Mol. Cell* **2015,** *57* (5), 936-947.
11. Wheeler, J. R.; Matheny, T.; Jain, S.; Abrisch, R.; Parker, R., Distinct stages in stress granule assembly and disassembly. *Elife* **2016,** *5*.
12. Kim, J.; Lee, H.; Lee, H. G.; Seo, P. J., Get closer and make hotspots: liquid-liquid phase separation in plants. *EMBO Rep* **2021,** *22* (5), e51656.
13. Patel, A.; Lee, H. O.; Jawerth, L.; Maharana, S.; Jahnel, M.; Hein, M. Y.; Stoynov, S.; Mahamid, J.; Saha, S.; Franzmann, T. M.; Pozniakovski, A.; Poser, I.; Maghelli, N.; Royer, L. A.; Weigert, M.; Myers, E. W.; Grill, S.; Drechsel, D.; Hyman, A. A.; Alberti, S., A Liquid-to-Solid Phase Transition of the ALS Protein FUS Accelerated by Disease Mutation. *Cell* **2015,** *162* (5), 1066-77.
14. Babinchak, W. M.; Surewicz, W. K., Liquid-Liquid Phase Separation and Its Mechanistic Role in Pathological Protein Aggregation. *J. Mol. Biol.* **2020,** *432* (7), 1910-1925.
15. Nguemaha, V.; Zhou, H. X., Liquid-Liquid Phase Separation of Patchy Particles Illuminates Diverse Effects of Regulatory Components on Protein Droplet Formation. *Sci. Rep.* **2018,** *8* (1), 6728.
16. Berry, J.; Weber, S. C.; Vaidya, N.; Haataja, M.; Brangwynne, C. P., RNA transcription modulates phase transition-driven nuclear body assembly. *Proc. Natl. Acad. Sci. U. S. A.* **2015,** *112* (38), E5237-45.
17. Emmanouilidis, L.; Esteban-Hofer, L.; Damberger, F. F.; de Vries, T.; Nguyen, C. K. X.; Ibanez, L. F.; Mergenthal, S.; Klotzsch, E.; Yulikov, M.; Jeschke, G.; Allain, F. H., NMR and EPR reveal a compaction of the RNA-binding protein FUS upon droplet formation. *Nat. Chem. Biol.* **2021,** *17* (5), 608-614.
18. Matsuo, M.; Kurihara, K., Proliferating coacervate droplets as the missing link between chemistry and biology in the origins of life. *Nat Commun* **2021,** *12* (1), 5487.
19. Wen, J.; Hong, L.; Krainer, G.; Yao, Q. Q.; Knowles, T. P. J.; Wu, S.; Perrett, S., Conformational Expansion of Tau in Condensates Promotes Irreversible Aggregation. *J. Am. Chem. Soc.* **2021,** *143* (33), 13056-13064.
20. Nel, A. E.; Madler, L.; Velegol, D.; Xia, T.; Hoek, E. M.; Somasundaran, P.; Klaessig, F.; Castranova, V.; Thompson, M., Understanding biophysicochemical interactions at the nano-bio interface. *Nat Mater* **2009,** *8* (7), 543-57.
21. O'Brien, M. N.; Jones, M. R.; Lee, B.; Mirkin, C. A., Anisotropic nanoparticle complementarity in DNA-mediated co-crystallization. *Nat Mater* **2015,** *14* (8), 833-9.
22. Agudo-Canalejo, J.; Lipowsky, R., Critical Particle Sizes for the Engulfment of Nanoparticles by Membranes and Vesicles with Bilayer Asymmetry. *ACS Nano* **2015,** *9* (4), 3704-3720.
23. Xue, Z.; Yan, C.; Wang, T., From Atoms to Lives: The Evolution of Nanoparticle Assemblies. *Adv. Funct. Mater.* **2019,** *29* (12), 1807658.
24. Yue, J.; Feliciano, T. J.; Li, W.; Lee, A.; Odom, T. W., Gold Nanoparticle Size and Shape Effects on Cellular Uptake and Intracellular Distribution of siRNA Nanoconstructs. *Bioconjug. Chem.* **2017,** *28* (6), 1791-1800.
25. Baranov, M. V.; Kumar, M.; Sacanna, S.; Thutupalli, S.; van den Bogaart, G., Modulation of Immune Responses by Particle Size and Shape. *Front. Immunol.* **2020,** *11*, 607945.
26. Guan, G.; Win, K. Y.; Yao, X.; Yang, W.; Han, M. Y., Plasmonically Modulated Gold Nanostructures for Photothermal Ablation of Bacteria. *Adv Healthc Mater* **2020**, e2001158.
27. Dreaden, E. C.; Alkilany, A. M.; Huang, X.; Murphy, C. J.; El-Sayed, M. A., The golden age: gold nanoparticles for biomedicine. *Chem. Soc. Rev.* **2012,** *41* (7), 2740-79.
28. Venkatesan, J.; Gupta, P. K.; Son, S. E.; Hur, W.; Seong, G. H., Silver-Based Hybrid Nanomaterials: Preparations, Biological, Biomedical, and Environmental Applications. *J. Cluster Sci.* **2022**.
29. Yu, K. K.; Li, K.; Qin, H. H.; Zhou, Q.; Qian, C. H.; Liu, Y. H.; Yu, X. Q., Construction of pH-Sensitive "Submarine" Based on Gold Nanoparticles with Double Insurance for Intracellular pH Mapping, Quantifying of Whole Cells and in Vivo Applications. *ACS Appl Mater Interfaces* **2016**.
30. Boisselier, E.; Astruc, D., Gold nanoparticles in nanomedicine: preparations, imaging, diagnostics, therapies and toxicity. *Chem. Soc. Rev.* **2009,** *38* (6), 1759-82.
31. Perezjuste, J.; Pastorizasantos, I.; Lizmarzan, L.; Mulvaney, P., Gold nanorods: Synthesis, characterization and applications. *Coord. Chem. Rev.* **2005,** *249* (17-18), 1870-1901.
32. Lohse, S. E.; Murphy, C. J., The Quest for Shape Control: A History of Gold Nanorod Synthesis. *Chem. Mater.* **2013,** *25* (8), 1250-1261.
33. Goncalves, A. S. C.; Rodrigues, C. F.; Moreira, A. F.; Correia, I. J., Strategies to improve the photothermal capacity of gold-based nanomedicines. *Acta Biomater.* **2020,** *116*, 105-137.
34. Elahi, N.; Kamali, M.; Baghersad, M. H., Recent biomedical applications of gold nanoparticles: A review. *Talanta* **2018,** *184*, 537-556.
35. Jana, N. R., Gram-scale synthesis of soluble, near-monodisperse gold nanorods and other anisotropic nanoparticles. *Small* **2005,** *1* (8-9), 875-882.
36. Scarabelli, L.; Sanchez-Iglesias, A.; Perez-Juste, J.; Liz-Marzan, L. M., A "Tips and Tricks" Practical Guide to

the Synthesis of Gold Nanorods. *J. Phys. Chem. Lett.* **2015,** *6* (21), 4270-9.
37. Wang, X.; Yang, D. P.; Huang, P.; Li, M.; Li, C.; Chen, D.; Cui, D., Hierarchically assembled Au microspheres and sea urchin-like architectures: formation mechanism and SERS study. *Nanoscale* **2012,** *4* (24), 7766-72.
38. Nehl, C. L.; Hafner, J. H., Shape-dependent plasmon resonances of gold nanoparticles. *J. Mater. Chem.* **2008,** *18* (21), 2415.
39. Soejima, T.; Morikawa, M. A.; Kimizuka, N., Holey gold nanowires formed by photoconversion of dissipative nanostructures emerged at the aqueous-organic interface. *Small* **2009,** *5* (18), 2043-7.
40. Nehl, C. L.; Liao, H.; Hafner, J. H., Optical Properties of Star-Shaped Gold Nanoparticles. *Nano Lett.* **2006,** *6* (4), 683-688.
41. Song, T.; Tang, L.; Tan, L. H.; Wang, X.; Satyavolu, N. S.; Xing, H.; Wang, Z.; Li, J.; Liang, H.; Lu, Y., DNA-Encoded Tuning of Geometric and Plasmonic Properties of Nanoparticles Growing from Gold Nanorod Seeds. *Angew. Chem. Int. Ed. Engl.* **2015,** *54* (28), 8114-8.
42. Michael J. Walsh; Steven J. Barrow; Wenming Tong; Alison M. Funston; Joanne Etheridge, Symmetry Breaking and Silver in Gold Nanorod Growth. *ACS Nano* **2015,** *9* (1), 715-724.
43. Tong, W.; Walsh, M. J.; Mulvaney, P.; Etheridge, J.; Funston, A. M., Control of Symmetry Breaking Size and Aspect Ratio in Gold Nanorods: Underlying Role of Silver Nitrate. *The Journal of Physical Chemistry C* **2017,** *121* (6), 3549-3559.
44. Mingzhao Liu; Guyot-Sionnest, P., Mechanism of Silver(I)-Assisted Growth of Gold Nanorods and Bipyramids. *The Journal of Physical Chemistry B* **2005,** *109*, 22192-22200.
45. Shiraki, K.; Mimura, M.; Nishinami, S.; Ura, T., Effect of additives on liquid droplets and aggregates of proteins. *Biophys Rev* **2020,** *12* (2), 587-592.
46. Zhang, Q.; Zhou, Y.; Villarreal, E.; Lin, Y.; Zou, S.; Wang, H., Faceted Gold Nanorods: Nanocuboids, Convex Nanocuboids, and Concave Nanocuboids. *Nano Lett.* **2015,** *15* (6), 4161-9.
47. Singh, G.; Agrawal, T.; Lesani, P.; Bisht, P. B.; Zreiqat, H., Tuning the size, concaveness, and aspect ratio of concave cubic gold nanoparticles produced with high reproducibility. *Materials Today Chemistry* **2022,** *23*, 100657.
48. Murakami, T.; Nakatsuji, H.; Morone, N.; Heuser, J. E.; Ishidate, F.; Hashida, M.; Imahori, H., Mesoscopic Metal Nanoparticles Doubly Functionalized with Natural and Engineered Lipidic Dispersants for Therapeutics. *ACS Nano* **2014,** *8* (7), 7370-7376.
49. Hamada, H.; Arakawa, T.; Shiraki, K., Effect of Additives on Protein Aggregation. *Curr. Pharm. Biotechnol.* **2009,** *10* (4), 400-407.
50. Tsumoto, K.; Umetsu, M.; Kumagai, I.; Ejima, D.; Philo, J. S.; Arakawa, T., Role of arginine in protein refolding, solubilization, and purification. *Biotechnol. Prog.* **2004,** *20* (5), 1301-8.
51. Arakawa, T.; Ejima, D.; Tsumoto, K.; Obeyama, N.; Tanaka, Y.; Kita, Y.; Timasheff, S. N., Suppression of protein interactions by arginine: A proposed mechanism of the arginine effects. *Biophys. Chem.* **2007,** *127* (1-2), 1-8.
52. Rajagopalan, K. V.; Fridovich, I.; Handler, P., Competitive Inhibition of Enzyme Activity by Urea. *J. Biol. Chem.* **1961,** *236* (4), 1059-1065.
53. Lin, Y.; Mori, E.; Kato, M.; Xiang, S.; Wu, L.; Kwon, I.; McKnight, S. L., Toxic PR Poly-Dipeptides Encoded by the C9orf72 Repeat Expansion Target LC Domain Polymers. *Cell* **2016,** *167* (3), 789-802 e12.
54. Liu, M.; Guyot-Sionnest, P., Mechanism of silver(I)-assisted growth of gold nanorods and bipyramids. *J. Phys. Chem. B* **2005,** *109* (47), 22192-200.
55. Koga, S.; Williams, D. S.; Perriman, A. W.; Mann, S., Peptide-nucleotide microdroplets as a step towards a membrane-free protocell model. *Nat. Chem.* **2011,** *3* (9), 720-4.
56. Nakashima, K. K.; Baaij, J. F.; Spruijt, E., Reversible generation of coacervate droplets in an enzymatic network. *Soft Matter* **2018,** *14* (3), 361-367.
57. Ura, T.; Tomita, S.; Shiraki, K., Dynamic behavior of liquid droplets with enzyme compartmentalization triggered by sequential glycolytic enzyme reactions. *Chem. Commun. (Camb.)* **2021,** *57* (93), 12544-12547.
58. Huang, X.; Jain, P. K.; El-Sayed, I. H.; El-Sayed, M. A., Plasmonic photothermal therapy (PPTT) using gold nanoparticles. *Lasers Med. Sci.* **2008,** *23* (3), 217-28.
59. Nobeyama, T.; Shigyou, K.; Nakatsuji, H.; Sugiyama, H.; Komura, N.; Ando, H.; Hamada, T.; Murakami, T., Control of Lipid Bilayer Phases of Cell-Sized Liposomes by Surface-Engineered Plasmonic Nanoparticles. *Langmuir* **2020,** *36* (26), 7741-7746.
60. Jauffred, L.; Samadi, A.; Klingberg, H.; Bendix, P. M.; Oddershede, L. B., Plasmonic Heating of Nanostructures. *Chem. Rev.* **2019,** *119* (13), 8087-8130.
61. Zhang, Q.; Han, L.; Jing, H.; Blom, D. A.; Lin, Y.; Xin, H. L.; Wang, H., Facet Control of Gold Nanorods. *ACS Nano* **2016,** *10* (2), 2960-74.

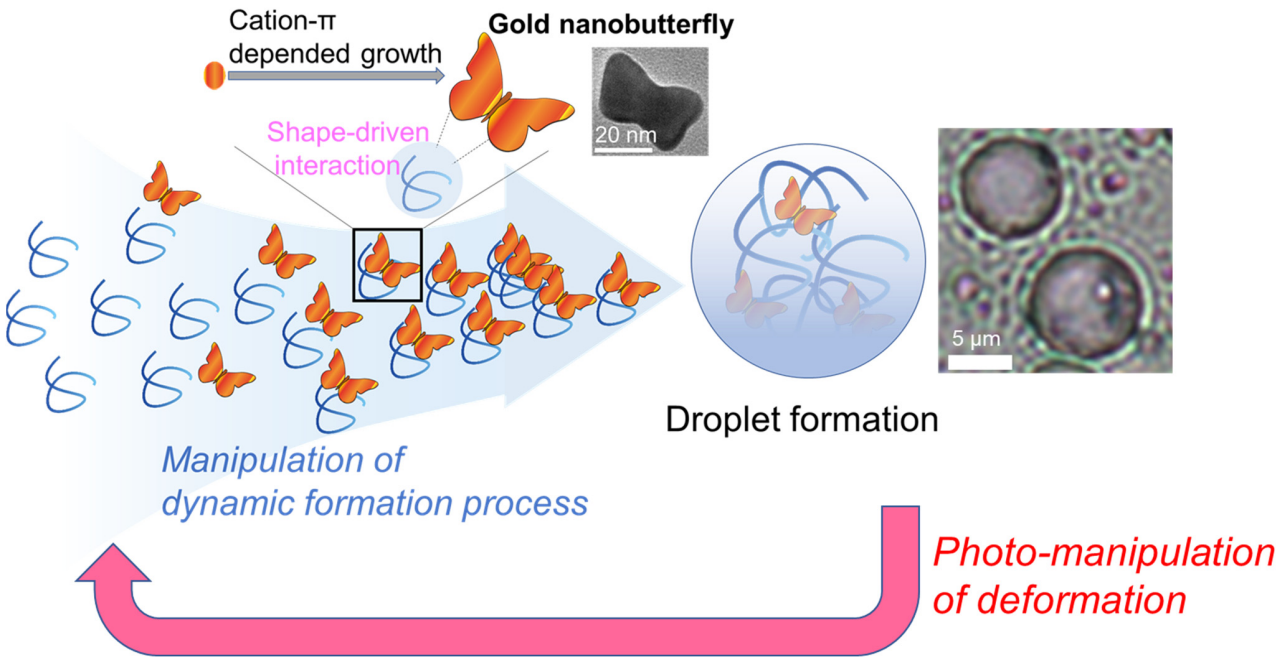
Cation-π
depended growth
Gold nanobutterfly
20 nm
Shape-driven
interaction
5 μm
Droplet formation
Manipulation of
dynamic formation process
Photo-manipulation
of deformation